THIN-FILM MAGNETLESS FARADAY ROTATORS FOR COMPACT HETEROGENEOUS INTEGRATED OPTICAL ISOLATORS

Dolendra Karki[1], Vincent Stenger[2], Andrea Pollick[2], Miguel Levy[1]

[1] Physics Department, Michigan Technological University, Houghton, Michigan 49931, U.S.A.

[2]SRICO, Inc., Columbus, Ohio 43235, U.S.A.

ABSTRACT

This report describes the fabrication, characterization and transfer of ultra-compact thin-film magnetless Faraday rotators to silicon photonic substrates. Thin films of magnetization latching bismuth-substituted rare-earth iron garnets were produced from commercially available materials by mechanical lapping, dice polishing and crystal-ion-slicing. Eleven-μm-thick films were shown to retain the $45°$ Faraday rotation of the bulk material to within $2°$ at $1.55\,\mu m$ wavelength without re-poling. Anti-reflection coated films evince 0.09 dB insertion loses and better than -20 dB extinction ratios. Lower extinction ratios than the bulk are ascribed to multimode propagation. Significantly larger extinction ratios are predicted for single-mode waveguides. Faraday rotation, extinction ratios and insertion loss tests on He-ion implanted slab waveguides of the same material yielded similar results. The work culminated with bond alignment and transfer of 7 μm-thick crystal-ion-sliced 50 x 480 μm^2 films onto silicon photonic substrates.

I. INTRODUCTION

The miniaturization of optical isolators and circulators has been actively pursued over the last several decades [1-3]. This effort has been spurred by a widespread industrial need, particularly in optical telecommunications, to protect laser sources from return light and back reflections in optical circuits [1-3]. Driving factors for this undertaking include the expected robustness of integrated circuits, improved functional reliability, batch fabrication economy, improved optical alignment and immunity to vibrations.

Magneto-optic methodologies to on-chip isolation have received considerable attention because of the nonreciprocal nature of the Faraday Effect and the magneto-optic nonreciprocal phase-shift effect [1-3]. Both these techniques require the application of a magnetic field to saturate the magnetization in the device. Magneto-optic garnet materials, most notably bismuth-, and cerium-substituted iron garnets have been used in on-chip prototypes. These are also the materials of choice and are extensively used in bulk isolators sold commercially presently.

Most of the work devoted to the development of compact on-chip isolators has focused on the design and fabrication of optical waveguide structures, such as Faraday rotators [4-6], Mach-Zehnder interferometers [7-9], ring resonators [10, 11], and other variants [12-14]. But the remaining issue of reducing the size or eliminating the magnetizing element,

be it permanent magnets or electromagnets, has not been addressed extensively [6, 15, 16]. In fact, it is the magnetizing element which accounts for a considerable part of the bulk of these devices at present. Prior work by one of the co-authors has addressed the integration of permanent magnet films in Faraday rotator waveguide structures [6, 15]. But no work has been reported on the complete elimination of the magnetizing element in micron-scale magneto-optic devices. It is this question that is addressed here.

In addition, this article also addresses the critical figures of merit in optical isolation, besides the elimination of magnet bulk, namely, insertion loss and isolation ratio. Isolation ratios compare the forward optical power transmitted by the device to the backward propagating light reaching the laser source. The results presented here show the lowest insertion losses achieved so far for miniaturized Faraday rotators, comparable to those in bulk isolators sold commercially, and are comparable to the best isolation ratios achieved with on-chip devices [1-3]. This superior performance stems from the high quality of the liquid-phase-epitaxially-grown (LPE) materials used in our work, and the processing techniques reported here. Of particular note is our use of crystal-ion-slicing, an ion-implantation-based technique to detach and transfer micron-scale-thick film samples from high-quality bulk materials that sidesteps the need for lattice-matched epitaxial growth on the optical platform [17, 18].

Liquid-phase-epitaxially-grown bismuth-substituted iron garnet mono-crystal materials are regularly used in technologically-important nonreciprocal photonic components, including optical isolators, circulators and switches. These materials are especially valued for their high-optical quality, particularly low-loss and large Faraday rotations in the infrared telecom wavelength range.

Latching Faraday-rotator LPE iron-garnets have the additional remarkable attribute that they do not require bias magnets for their operation. This significant feature makes it possible to greatly reduce rotator device size relative to designs that require an external applied magnetic field. At $1.55\,\mu m$ -wavelength they typically display 0.43 dB/cm optical absorption and 938 deg/cm (1745 rad/m) Faraday rotation, making them ideal nonreciprocal device materials.

The key to magnetless operation resides in the composition of the garnet. A saturated magnetic state without bias magnets is achieved through maximizing the incorporation of europium (Eu) in order to reduce the saturation magnetization of the garnet without creating a compensation point [19, 20]. The nominal composition of the garnet is $Bi_X(Eu_ZHo_{1-Z})_{3-X}Fe_{5-Y}Ga_YO_{12}$ per formula unit.

These materials are grown on (111)-oriented single-crystal Ca/Mg/Zr-substituted gadolinium gallium garnet (CMZ-GGG) substrates and their integration into silicon or into other non-compatible platforms has not been demonstrated. As grown, their magnetization axis is normal to the plane of the film (Fig. 1(a)). Therefore the on-chip integration of these Faraday rotators into alternative platforms requires post-LPE-growth manufacturing to form a new thin-film-plane. Its normal should be perpendicular to the growth direction, as in Fig. 1(b). The optical propagation axis must be along the magnetization direction.

This manuscript was accepted by J. Appl. Phys. Click here to see the version of record.

This letter reports on the fabrication of such films and their integration into silicon-on-insulator (SOI) and other platforms. It is shown that processed films via mechanical thin-down lapping retain their magnet-less latching character and their original bulk Faraday rotations without re-poling to within experimental error. Film-transfer onto silicon photonic chips by crystal-ion-slicing is also described. This latter technique was originally introduced by one of the co-authors several years ago for non-latching iron garnets and is here extended to latching materials [17]. Tests show that ion-implanted samples exhibit minimal changes in magneto-optical properties from the bulk, and excellent optical transmission, as detailed below.

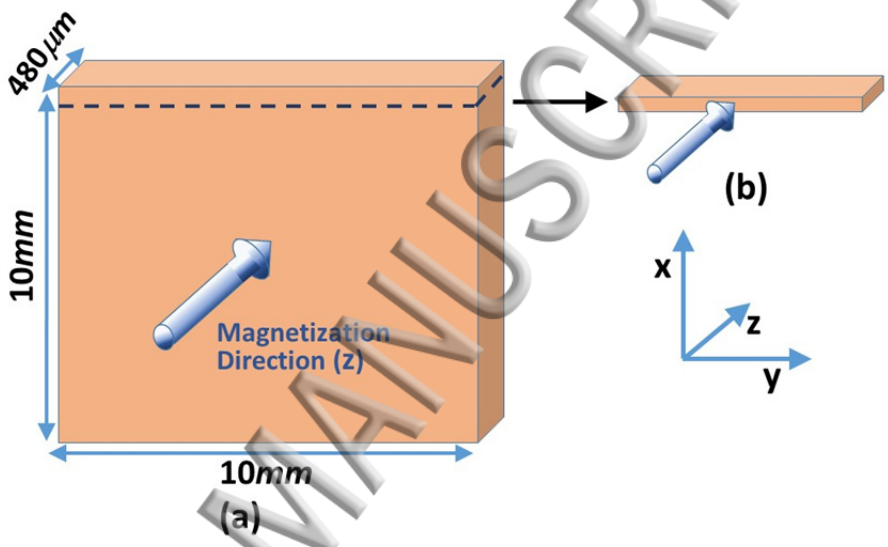

FIG. 1. Geometry of the latching Faraday rotators. The magnetization direction is normal to the large faces. (Drawing not to scale).

II. PROCESSING AND MAGNETO-OPTICAL PROPERTIES OF MECHANICALLY PROCESSES THIN-FILMS

Anti-reflection-coated $480\,\mu m$ -thick, $10\times 10\,mm^2$ latching Faraday-rotator pieces were procured from Integrated Photonics, Inc. These materials retain their magnetization without externally applied magnetic fields for their operation. The pieces were cut to produce $45°$ rotations at normal incidence. Faraday rotation and insertion loss measurements on the as-procured samples at $1.55\,\mu m$ wavelength performed in our laboratory yielded $44.3°\pm 1.3°$ and 0.02 dB, respectively.

Strips measuring $2mm\times 10mm\times 480\,\mu m$ were cut off from the original pieces, with the magnetization direction along the $480\,\mu m$ – long side. The $2mm\times 10mm$ facets remained anti-reflection-coated on both sides. These strips were crystal-wax-bonded to silicon platforms and the $2mm$ side was thinned down via diamond-film lapping. The finest diamond particle size used for polishing was $0.25\,\mu m$. Films of three different thicknesses

This manuscript was accepted by J. Appl. Phys. Click here to see the version of record.

$11\mu m$, $50\mu m$ and $300\mu m$ were produced. Figures 2 shows scanning-electron-micrographs (SEM) of the first two types.

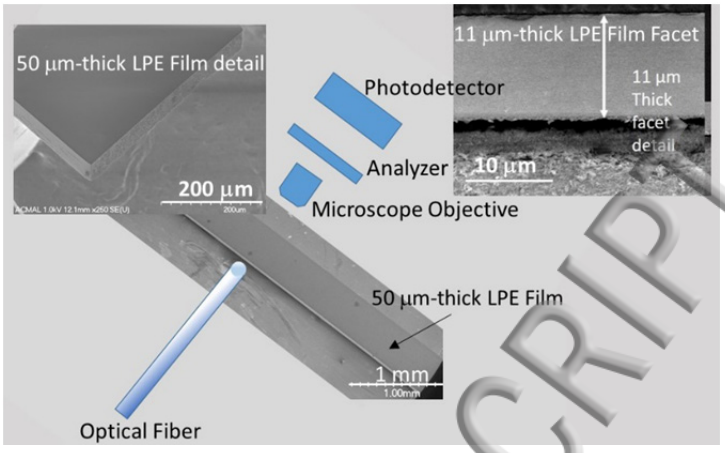

FIG. 2. $50\mu m$-thick film cross-section SEM images, with schematic depiction of the optical fiber and detection components used for Faraday rotation testing. $11\mu m$-thick film facet cross-section SEM image.

Figure 3 depicts the Faraday rotation testing setup used to characterize the processed films. A lensed fiber couples linearly polarized light into the Faraday rotator. The light is vertically confined in the film but diffracts laterally, as evidenced by the output image (Fig. 3 inset) from the $11\mu m$-thick sample. A Glan-Thomson polarizer allows us to analyze the angular-dependence of the output polarization.

Faraday rotations, insertion losses and extinction ratios for the three mechanically polished films, all without re-poling, are shown in Table I. Extinction ratios are defined as the power ratios between minimum and maximum transmission powers for the Faraday rotations, in dB. For the purposes of this table, we define Faraday rotation as the direction of the semi-major axis of the rotated polarization ellipse. The rotations are exhibited for opposite propagation directions, where forward propagation is defined in the magnetization direction. Uncertainties correspond to one standard deviation from average values taken over several measurements in each case. Also displayed in the table is the response for the bulk material. The polarization response of the $11\mu m$-thick film as a function of analyzer angle for one of these measurements is shown in Fig. 4.

This manuscript was accepted by J. Appl. Phys. Click here to see the version of record.

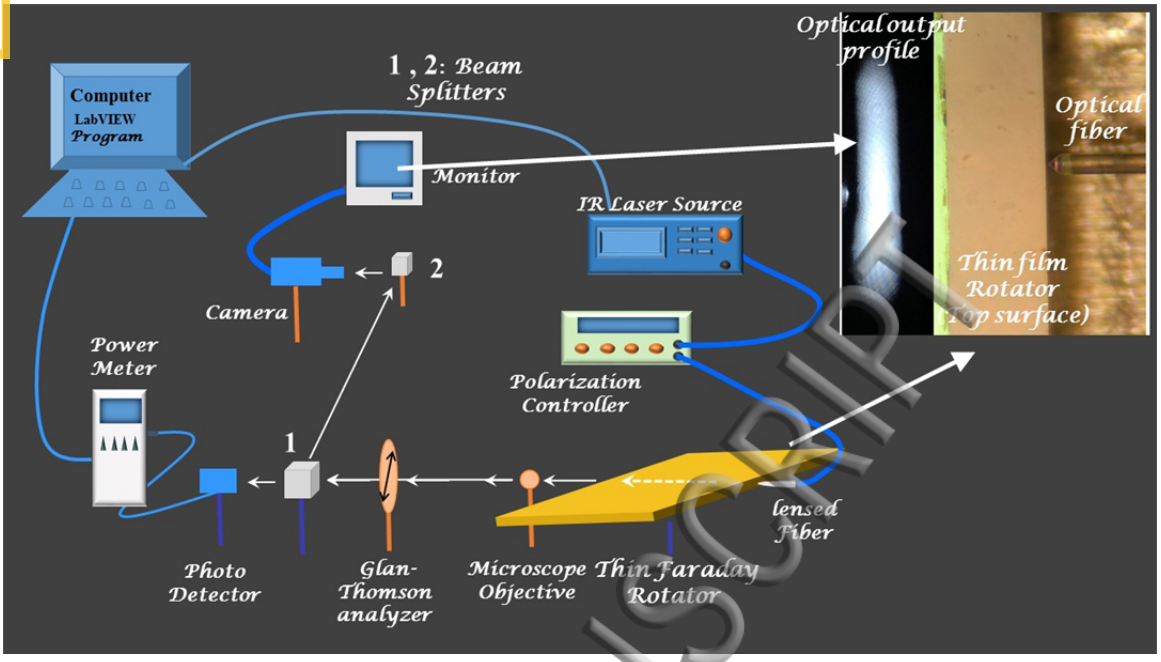

FIG. 3. Testing set-up for measuring Faraday rotation in the latching iron garnet film samples. The inset shows the diffracted output image from the 11μm-thick film. It also shows a top view of the lensed fiber tip and the top surface of the film.

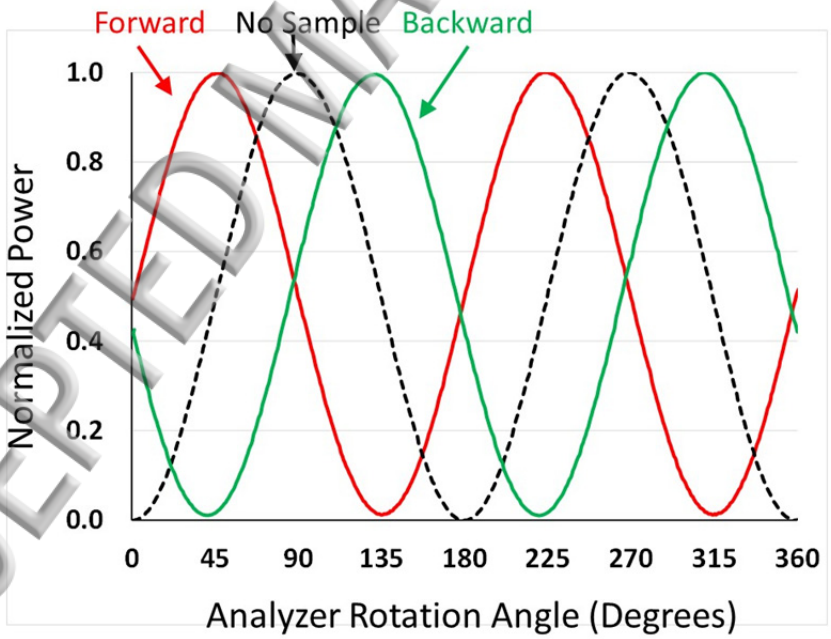

FIG. 4. 360^0 analyzer rotation scans with and without 11 μm -thick sample in the beam path.

TABLE I. Faraday rotations, extinction ratios and insertion losses for mechanically polished films without re-poling.

Sample	Forward FR	Backward FR	Extinction	Insertion Loss
Bulk	44.7° ± 0.9°	44.5° ± 0.6°	< -30 dB	0.02 dB
300 μm –thick	45.2° ± 1.0°	44.3° ± 0.9°	< -30 dB	NA
50 μm –thick	45.6° ± 0.8°	44.2° ± 0.5°	< -30 dB	NA
11 μm –thick	46.7° ± 2.1°	41.9° ± 1.9°	–20.5 ± 2.0 dB	0.09 ± 0.01 dB

III. MODE BIREFRINGENCE AND FARADAY ROTATION

Slab waveguides introduce a disparity between transverse-electric (TE) and transverse magnetic (TM) mode indices (linear birefringence) in addition to the existing circular birefringence inherent in the Faraday effect. As a consequence the output polarization acquires some degree of ellipticy and suffers rotational departures from that of the bulk material. However, it was found that this effect is negligible for $300\,\mu m$- and $50\,\mu m$-thick films, and relatively small for $11\,\mu m$-thick films.

In the presence of linear birefringence, the otherwise circularly-polarized counter-gyrating normal modes of the Faraday rotator become elliptically polarized. And their phase difference after any given propagation length L changes as well. Given an intrinsic Faraday rotation angle per unit length θ_F and linear birefringence between TE and TM modes $n_{TE} - n_{TM}$, the phase mismatch between counter-gyrating elliptical normal modes after a distance L becomes

$$\phi = 2L\sqrt{{\theta_F}^2 + \left[\frac{\pi}{\lambda}(n_{TE} - n_{TM})\right]^2}\ . \qquad (1)$$

λ is the free-space wavelength.

Taking into account the calculated geometrical birefringence $n_{TE} - n_{TM}$ for an $11\,\mu m$-thick iron-garnet slab with crystal bond bottom cladding yields the following polarization rotations and extinction ratios for the first four waveguide modes (Table II). These are obtained making use of the calculated phase mismatched from Eq. 1. We assume $\theta_F L = 45°$, film index = 2.35, bottom cladding index = 1.5277, and $\lambda = 1.55\,\mu m$.

Notice that the observed $11\,\mu m$-thick film extinction ratio displayed in Table I is consistent with the detrimental presence of higher-order modes in the slab waveguide. Other effects such as film-surface roughness and stress birefringence cannot be completely ruled out. A single-mode structure, achievable through additional processing (thinning and patterning) should, theoretically, yield extinction ratios higher than -30 dB, as predicted in Table II.

IV. POLARIZATION ROTATION TESTS ON SLAB WAVEGUIDES FORMED BY ION IMPLANTATION

Crystal ion slicing proceeds via energetic He-ion implantation into metal oxides [17, 18]. In this work, the ions were accelerated to an energy of 3.5 MeV and deposited at a dose of 5×10^{16} cm^{-2}. Rapid thermal annealing (RTA) under nitrogen flow for 30s in the temperature range 700 °C to 800 °C produced best results.

A low-refractive-index sacrificial layer due to the implantation forms below the surface that is then etched away to detach the top film from the rest of the sample. This sacrificial layer can act as a cladding layer for slab waveguiding prior to detachment.

TABLE II. Calculated polarization rotations and extinction ratios for the first four waveguide modes of an $11\mu m$-thick iron-garnet slab at $\lambda = 1.55\mu m$.

Waveguide Mode	$n_{TE} - n_{TM}$	Polarization Rotation	Extinction Ratio
Fundamental	0.000025	45.17°	-34.0 dB
First	0.000103	45.30°	-23.7 dB
Second	0.000231	45.50°	-15.9 dB
Third	0.000414	45.90°	-11.7 dB

The Faraday rotation and insertion loss of linearly-polarized light passing through these slab waveguides were characterized for different post-implantation rapid-thermal-annealing (RTA) preparation conditions. It was found that the magneto-optic response depended on RTA, approaching bulk material response at higher tested annealing temperatures. The output intensity profile after propagation is shown in the inset in Fig.5. Butt coupling from the lensed fiber onto the anti-reflection (AR) coated facet of the slab waveguide is also shown.

A comparison of the magneto-optical response in the ion-implanted slab waveguides with mechanically-thinned-down films evinces a more pronounced polarization ellipticity and somewhat larger departures from bulk Faraday rotation in the former. These more pronounced departures from bulk behavior in the ion-implanted slabs are consistent with a smaller waveguide thickness and the presence of high-order waveguide modes. Table III compares the performance in these two types of waveguides. The polarization ellipticity amelioration at higher RTA temperatures, referred to before, is also consistent with implantation-damage repair and segregation of residual crystal defects away from the waveguide core and towards the sacrificial layer. Figure 6 shows 360^0 analyzer rotation scans with and without the ion-implanted sample in the beam path, without re-poling.

TABLE III. Comparison of the magneto-optical response of ion-implanted slab waveguides with mechanically-thinned-down films.

Waveguide	Forward FR	Backward FR	Extinction	Insertion Loss
11 μm	46.7° ± 2.1°	41.9° ± 1.9°	–20.5 ± 2.0 dB	0.09 ± 0.01 dB
8 μm, Implanted	44°	40.7°	–17 dB	0.12 ± 0.01 dB

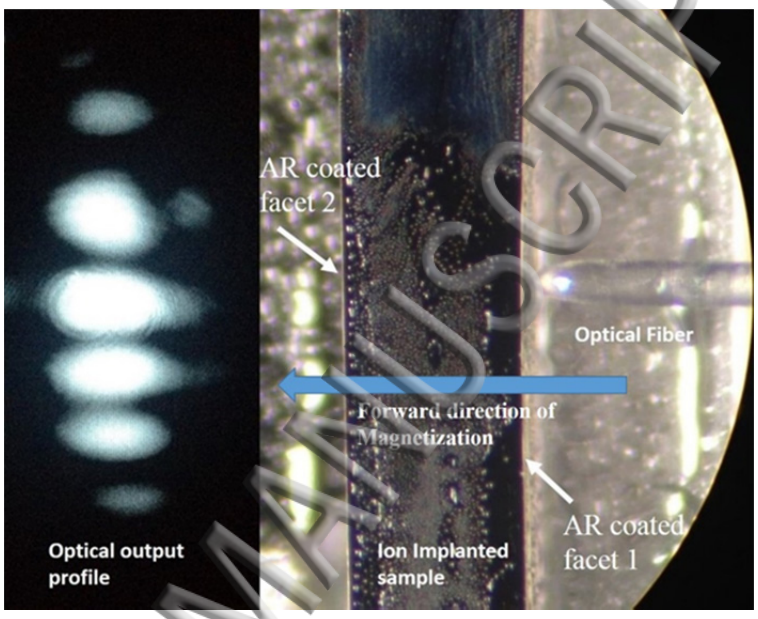

FIG. 5. Fiber launch configuration and mode profile for the ion implanted sample.

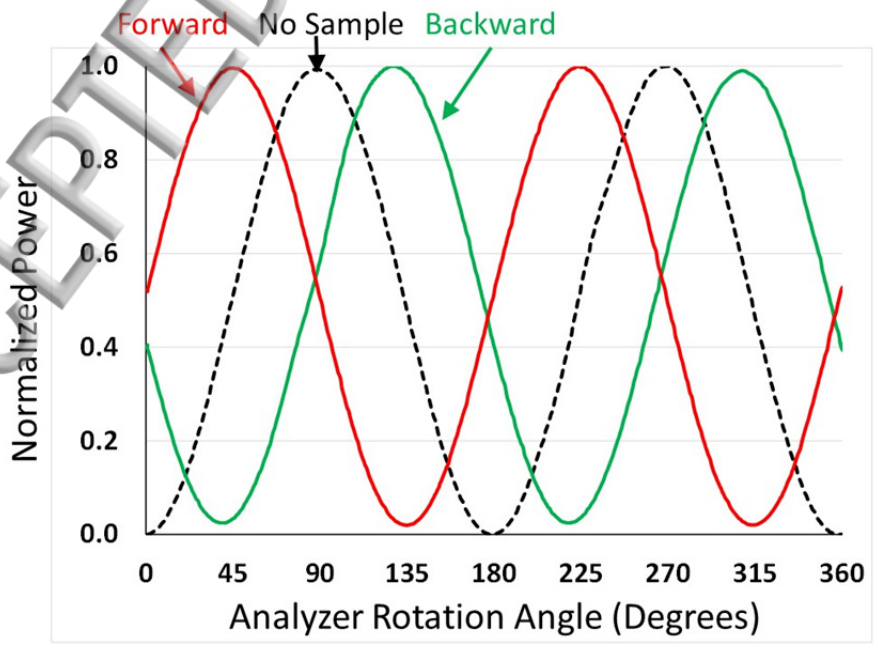

FIG. 6. 360^0 polarizer rotation scans with and without the sample in the beam path (No external magnetizing field). Data at $1.55\mu m$ wavelength.

Table IV exhibits the calculated departures from intrinsic Faraday rotation and power extinction ratios in $8\mu m$-thick slab waveguides as a result of mode birefringence. These results are consistent with the more pronounced departures as compared to the $11\mu m$-thick film. Insertion loss data in the ion-implanted slab waveguide was also measured at $1.55\mu m$ wavelength and found to be 0.12 ± 0.01 dB, slightly higher than the 0.09 ± 0.01 dB in the unimplanted sample (Table III). We tentatively ascribe this higher optical loss to residual post-anneal implantation-induced lattice damage in the core and cladding lattice defects in the optical waveguide.

TABLE IV. Calculated slab waveguide mode polarization-rotation departures from 45° (semi-major axis of polarization ellipse) in Faraday rotator due to mode birefringence. Slab and substrate refractive indices are assumed to be 2.35 and 1.95, respectively Slab thickness is $8\mu m$.

Waveguide Mode	Departure from 45°	Power Extinction Ratio
Fundamental	±0.4°	-28.5 dB
First	±0.5°	-15.9 dB
Second	±3.4°	-9.5 dB
Third	±10.4°	-4.6 dB

V. CRYSTAL-ION SLICING OF MAGNETLESS THIN-FILM FARADAY ROTATORS

Crystal-ion-slicing involves the ion implantation of energetic light ions to generate a sacrificial damage layer below the sample surface [17, 18]. This induces differential etching that undercuts the top layer when the sample is immersed in phosphoric acid to release the film. Rapid thermal annealing prior to etching repairs residual damage due to the ion trajectories above the sacrificial layer and enhances the differential etch rate with the sacrificial layer.

Prior work has shown crystal ion-sliced transfer of magnetic garnet films onto GaAs platforms [17]. Here a similar process was used to demonstrate the transfer of bias-free latching iron garnet films onto temporary handle substrates and characterize their Faraday rotation and insertion losses after ion-implantation prior to slicing. Future work will characterize their magneto-optic properties after full transfer.

Latching Faraday rotator samples were prepared for ion implantation to produce in-plane magnetized crystal-ion-sliced films, with magnetization axis along the propagation direction, as in Fig. 1. The as-received 10 mm x 10 mm x $480\mu m$ samples were cut into strips 10 mm x 1 mm x $480\mu m$ using a precision dice polishing process. Strips were then

This manuscript was accepted by J. Appl. Phys. Click here to see the version of record.

mounted for implantation normal to the10 mm x 480 μm face in order to form optical slab waveguides for Faraday rotation and absorption loss measurements prior to wet-etch and release of the films.

After implant, additional dice polish trenching of the implanted surface was done to form 50 μm wide rectangular features of various lengths from 100 μm to 480 μm. After bonding to a temporary handle wafer, crystal-ion slicing was done by wet etching to transfer the iron garnet films to the handle wafer. Figure 7 shows arrays of transferred films on a temporary handle wafer.

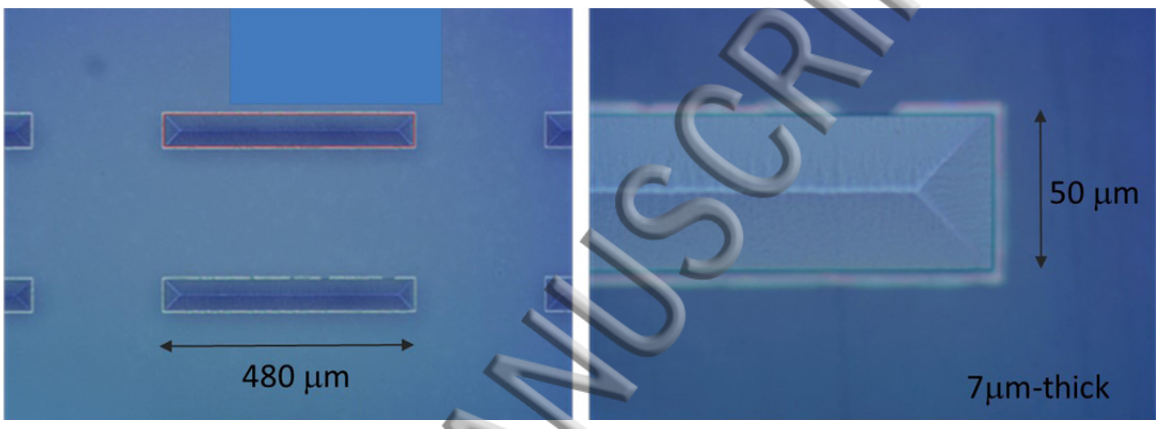

FIG. 7. Magnetless iron garnet films on temporary handle substrate after ion slicing. Detail on the right panel.

VI. TRANSFER TO Si PHOTONIC SUBSTRATES

Temporary mounted sliced magnetless iron garnet films of 7 μm thickness were bond-aligned and transferred to silicon photonic substrate by permanent adhesive bonding. An example of a bond aligned film is shown in Fig. 8. The film may be made to vertically couple to the underlying silicon waveguide by evanescent, reverse taper, grating, or other coupling methods. Alternatively, the film may be aligned and placed in a pre-milled slot in the silicon photonic substrate.

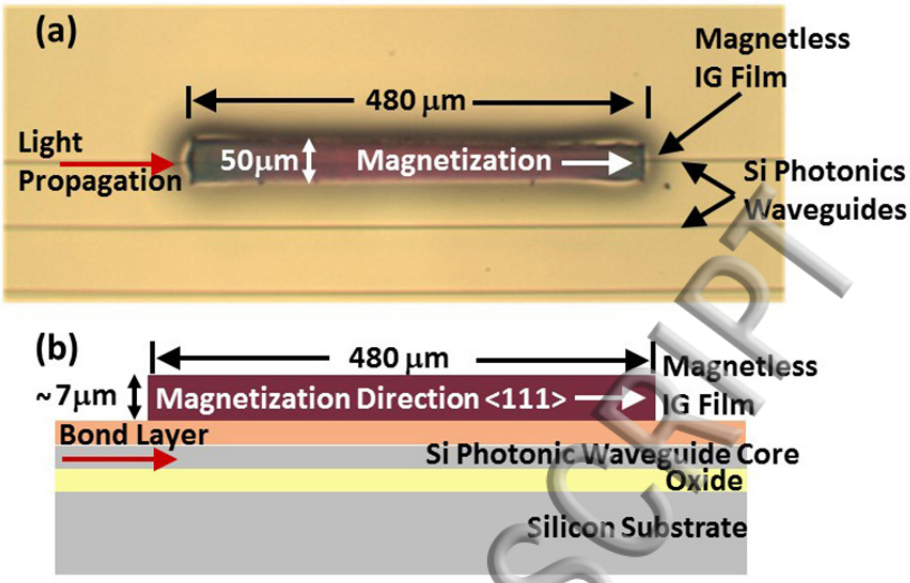

FIG. 8. Magnetless iron garnet (IG) film bond-align transferred to a silicon photonic substrate (a) top microscope image of bond-aligned film and (b) side view illustration showing the various material layers.

VII. CONCLUSIONS

In this work, fabrication, characterization and transfer of thin-film magnetless Faraday rotators to silicon photonic substrates has been demonstrated. Faraday rotations remain within 2° of bulk performance in 45° rotators, with extinction ratios better than -20 dB and insertion losses lower at 0.09 dB for 11μm-thick films. Departures from better than -30 dB bulk performance are ascribed mainly to the presence of high-order waveguide modes in the films and can be eliminated via single-mode structures. The magnetless film processing methodology developed in this work may be used to produce compact and high performance heterogeneous integrated isolators and circulators in silicon photonic substrates or in other semiconductor photonic platforms.

ACKNOWLEDGMENTS

This material is based on research sponsored by the Air Force Research Laboratory under contract number FA865016M5026. The U.S. Government is authorized to reproduce and distribute reprints for Governmental purposes notwithstanding any copyright notation thereon. DK thanks Michigan Tech's Physics Department for support.

REFERENCES

1. B. J. H. Stadler, T. Mizumoto, "Integrated Magneto-Optical Materials and Isolators: A Review," IEEE Photonics Journal **6**, 0600215 (2014).

2. T. Mizumoto, R. Takei, and Y. Shoji, "Waveguide Optical Isolators for Integrated Optics," IEEE J. of Quantum Electronics **48**, 252-260 (2012).

3. M. Levy, "The On-Chip Integration of Magnetooptic Waveguide Isolators," IEEE J. of Selected Topics in Quantum Electronics **8**, 1300-1306 (2002).

4. R. Wolfe, V. J. Fratello, and M. McGlashan-Powell, "Thin-film garnet materials with zero birefringence for magneto-optic waveguide devices," J. Appl. Phys. **63**, 3099–3103 (1988).

5. R. Wolfe, R. A. Lieberman, V. J. Fratello, R. E. Scotti, and N. Kopylov, "Etch-tuned ridged waveguide magneto-optic isolator," Appl. Phys. Lett. 56 426–428 (1990).

6. M. Levy, R. M. Osgood, Jr., H. Hegde, F. J. Cadieu, R. Wolfe, and V. J. Fratello, "Integrated Optical Isolators with Sputter-Deposited Thin-Film Magnets," IEEE Phot. Technol. Lett. **8**, 903-905 (1996).

7. J. Fujita, M. Levy, R. M. Osgood, Jr., L. Wilkens, and H. Dötsch, "Waveguide Optical Isolator Based on Mach-Zehnder Interferometer," Appl. Phys. Lett. **76**, 2158-2160 (2000).

8. Y. Shoji, T. Mizumoto, H. Yokoi, I-Wei Hsieh, and R. M. Osgood, Jr., "Magneto-optical isolator with silicon waveguides fabricated by direct bonding," Appl. Phys. Lett. **92**, 071117 (2008).

9. S. Ghosh, S. Keyvaninia, Y. Shoji, W. Van Roy, T. Mizumoto, G. Roelkens, and R. G. Baets, "Compact Mach–Zehnder Interferometer Ce:YIG/SOI Optical Isolators," IEEE Phot. Technol. Lett. **24**, 1653-1656 (2012).

10. M.-C. Tien, T. Mizumoto, P. Pintus, H. Kromer, and J. E. Bowers, "Silicon Ring Isolators with Bonded Nonreciprocal Magneto-Optic Garnets," Opt. Exp. **19**, 11740-11745 (2011).

11. L. Bi, J. Hu, P. Jiang, D. H. Kim, G. F. Dionne, L. C. Kimerling, and C. A. Ross, "On-chip Optical Isolation in Monolithically Integrated Nonreciprocal Optical Resonators," Nature Photonics **5**, 758–762 (2011).

12. H. Dammann, E. Pross, G. Rabe, andW. Tolksdorf, "45º Waveguide Isolators with Phase Mismatch," Appl. Phys. Lett. **56**, 1302–1304 (1990).

13. J. M. Hammer, J. H. Abeles, and D. J. Channin, "Polycrystalline-Metal-Ferromagnetic Optical Waveguide Isolator (POWI) for monolithic-integration with diode-laser devices," IEEE Photon. Technol. Lett. **9**, 631–633 (1997).

14. T. Shintaku, "Integrated optical isolator based on efficient nonreciprocal radiation mode conversion," Appl. Phys. Lett. **73**, 1946–1948 (1998).

15. M. Levy, I. Ilic, R. Scarmozzino, R. M. Osgood Jr., R. Wolfe, C. J. Gutierrez, and G. Prinz, "Thin-film-magnet magnetooptic waveguide Isolator," IEEE Photon. Technol. Lett., **5**, 198–200 (1993).

16. H. Lira, Z. Yu, S. Fan, and M. Lipson, "Electrically Driven Nonreciprocity Induced by Interband Photonic Transition on a Silicon Chip," Phys. Rev. Lett. **109**, 033901 (2012).

17. M. Levy, R. M. Osgood, Jr., A. Kumar, and H. Bakhru, "Epitaxial Liftoff of Thin Oxide Layers: Yttrium Iron Garnets onto GaAs," Appl. Phys. Lett. **71**, 2617 (1997).

18. M. Levy, R. M. Osgood, Jr., R. Liu, L. E. Cross, G. S. Cargill III, A. Kumar, and H. Bakhru, "Fabrication of Single-Crystal Lithium Niobate Films by Crystal Ion Slicing," Appl. Phys. Lett. **73**, 2293 (1998).

19. C. D. Brandle, Jr., V. J. Fratello, S. J. Licht, "Article Comprising a Magneto-Optic Material Having Low Magnetic Moment," US Patent 5,608,570 (1997).

20. R. R. Abbott, V. J. Fratello, S. J. Licht, I. Mnushkina, "Article Comprising a Faraday Rotator that Does Not Require a Bias Magnet," US Patent 6770223 B1 (2004).

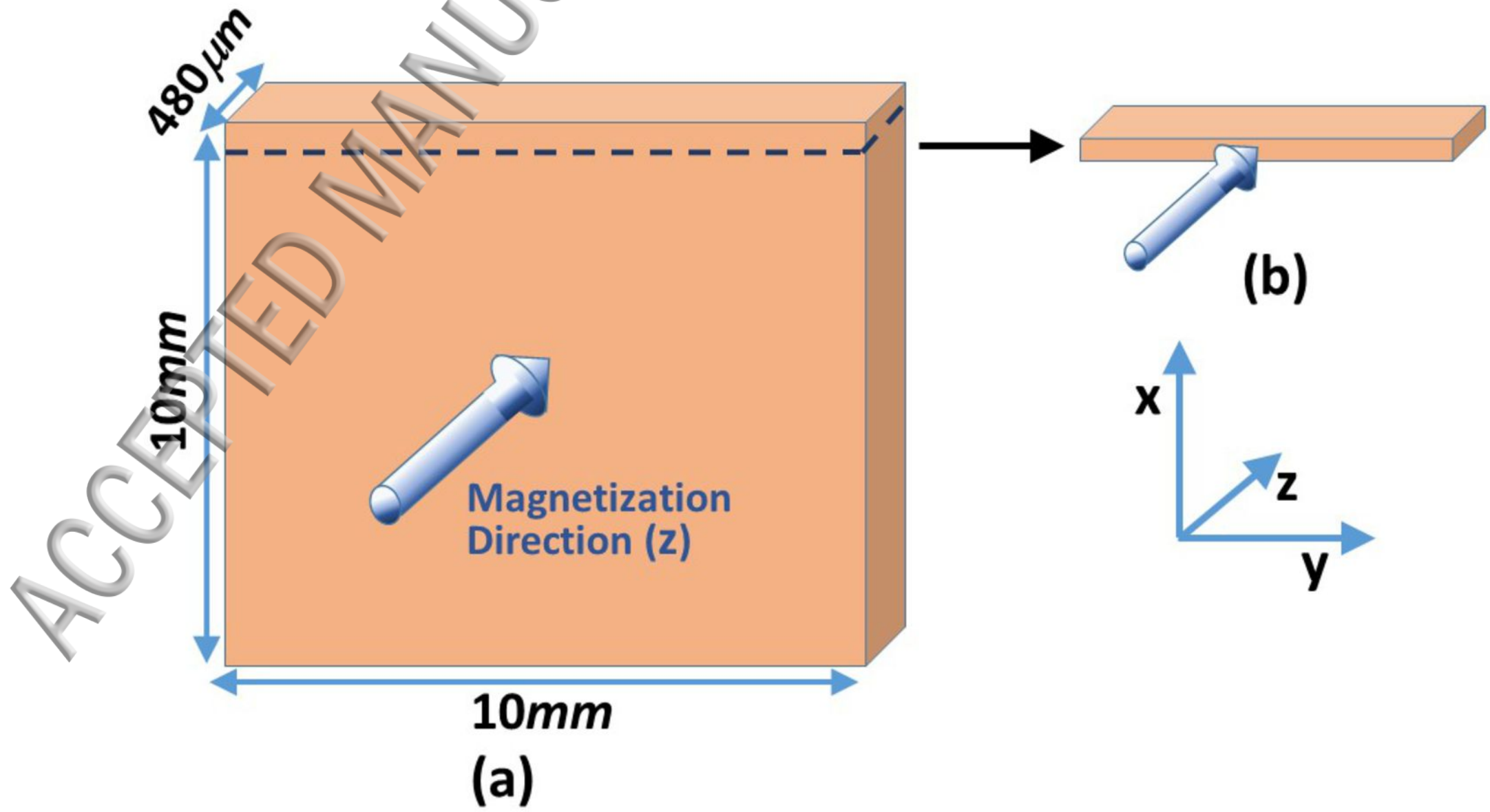

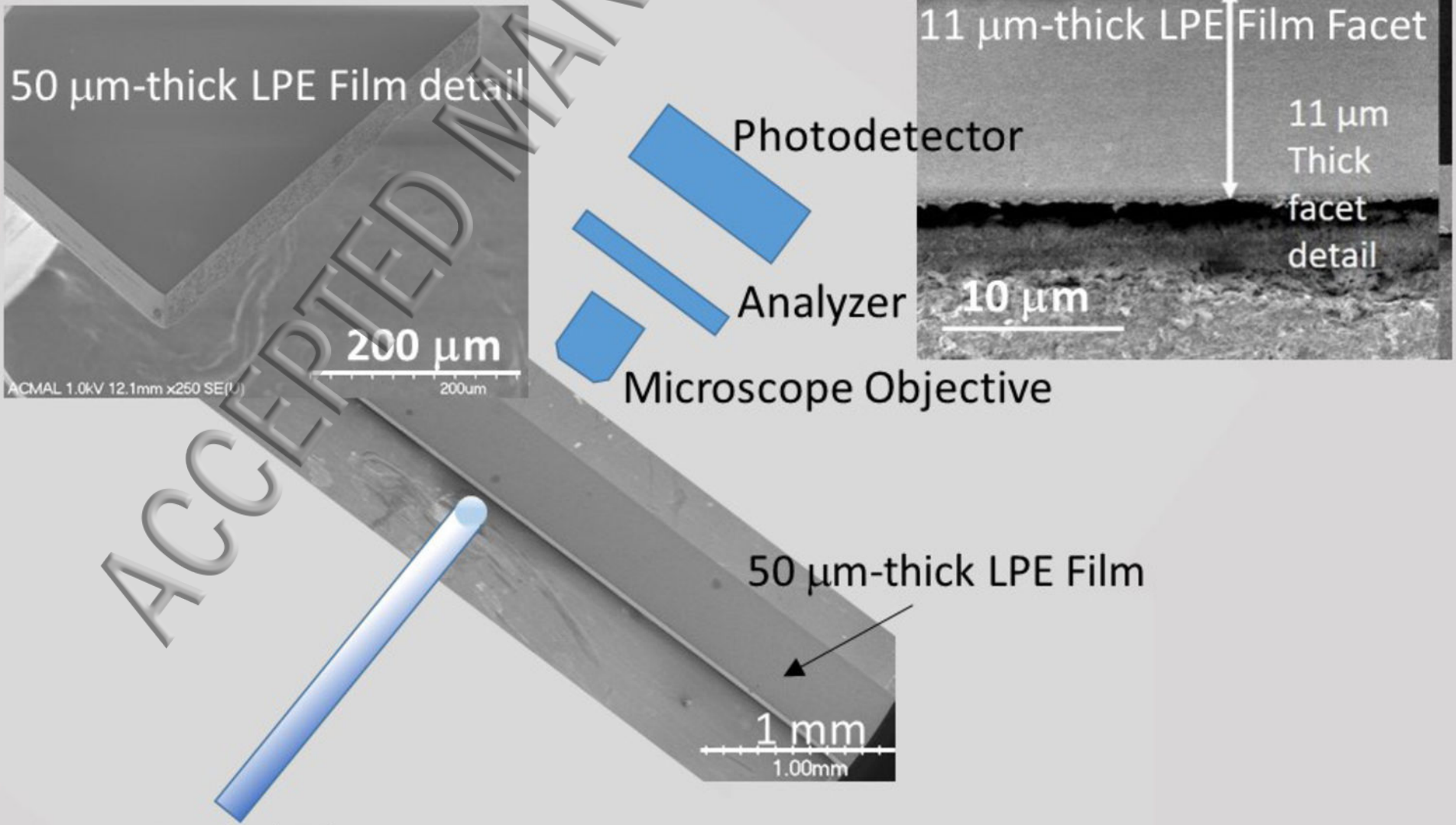

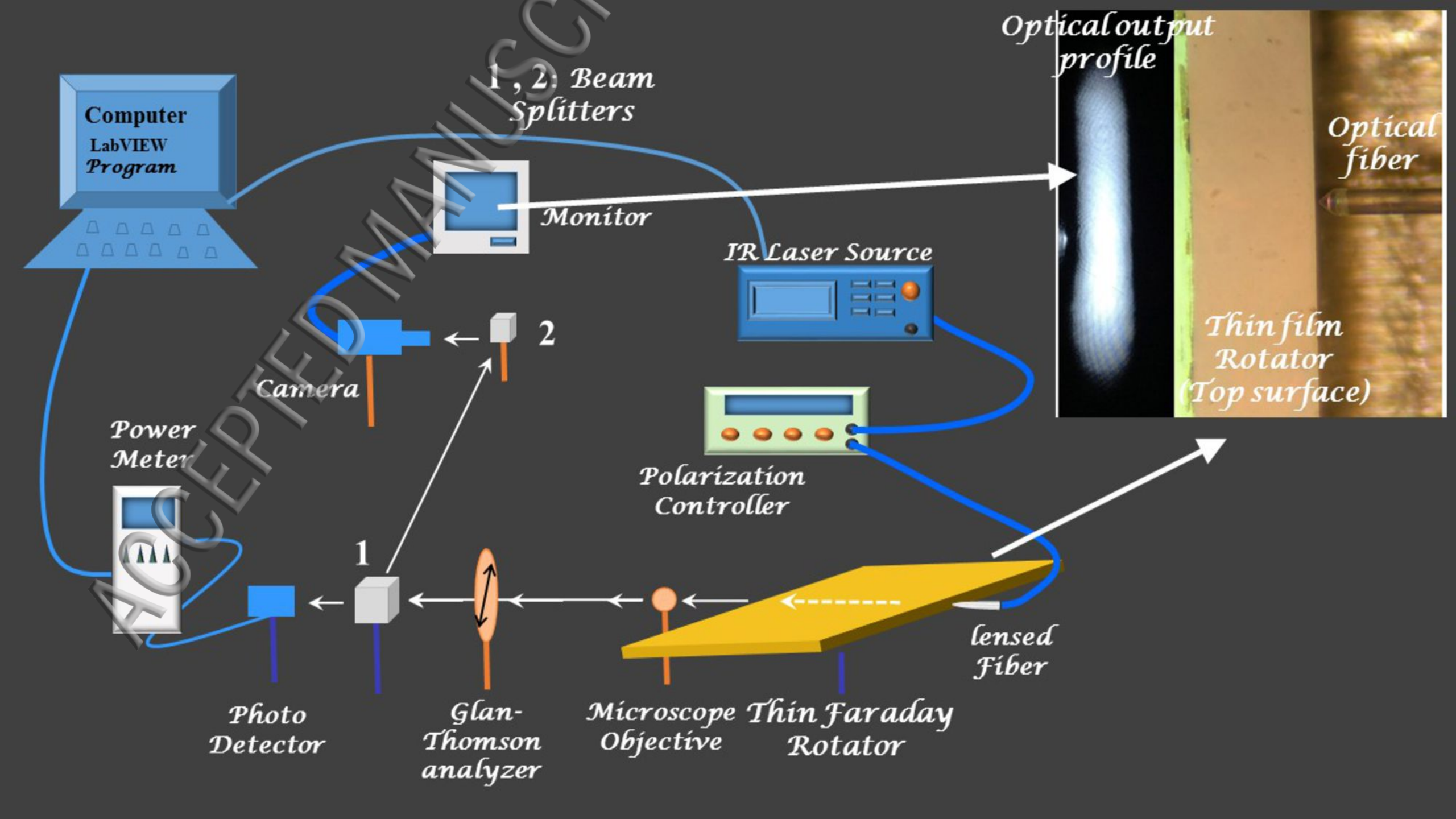

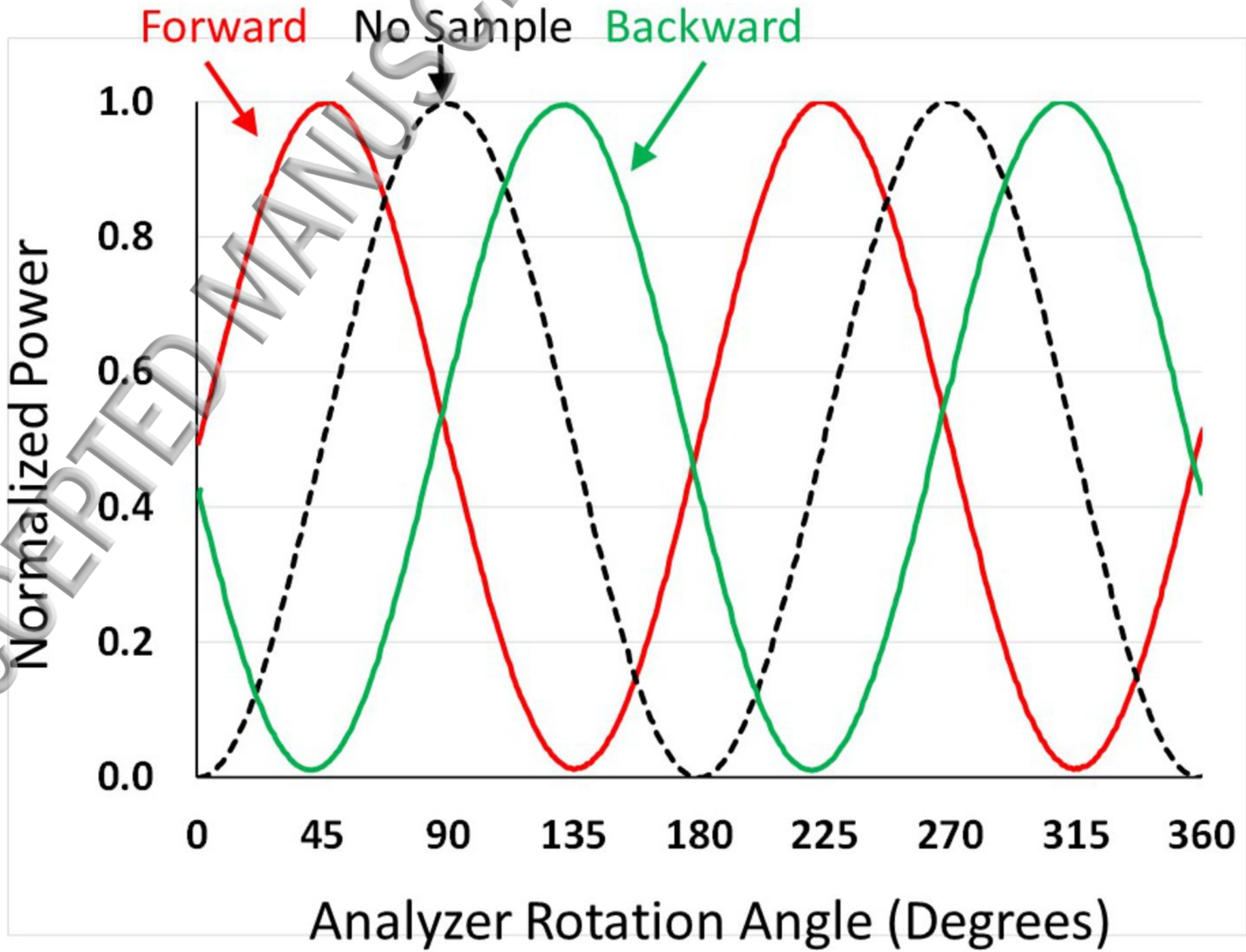

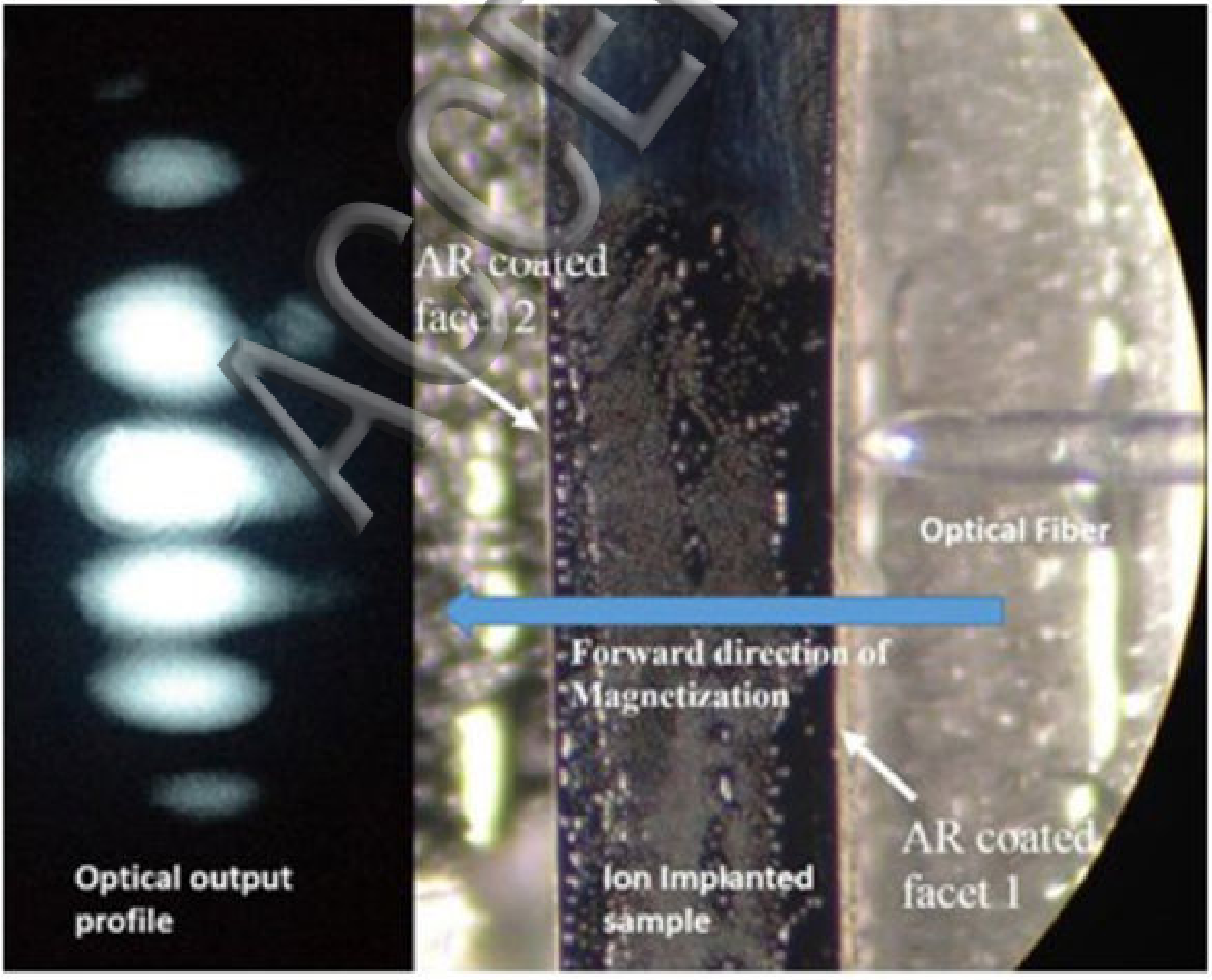
AR coated
facet 2
Optical Fiber
Forward direction of
Magnetization
AR coated
facet 1
Optical output
profile
Ion Implanted
sample

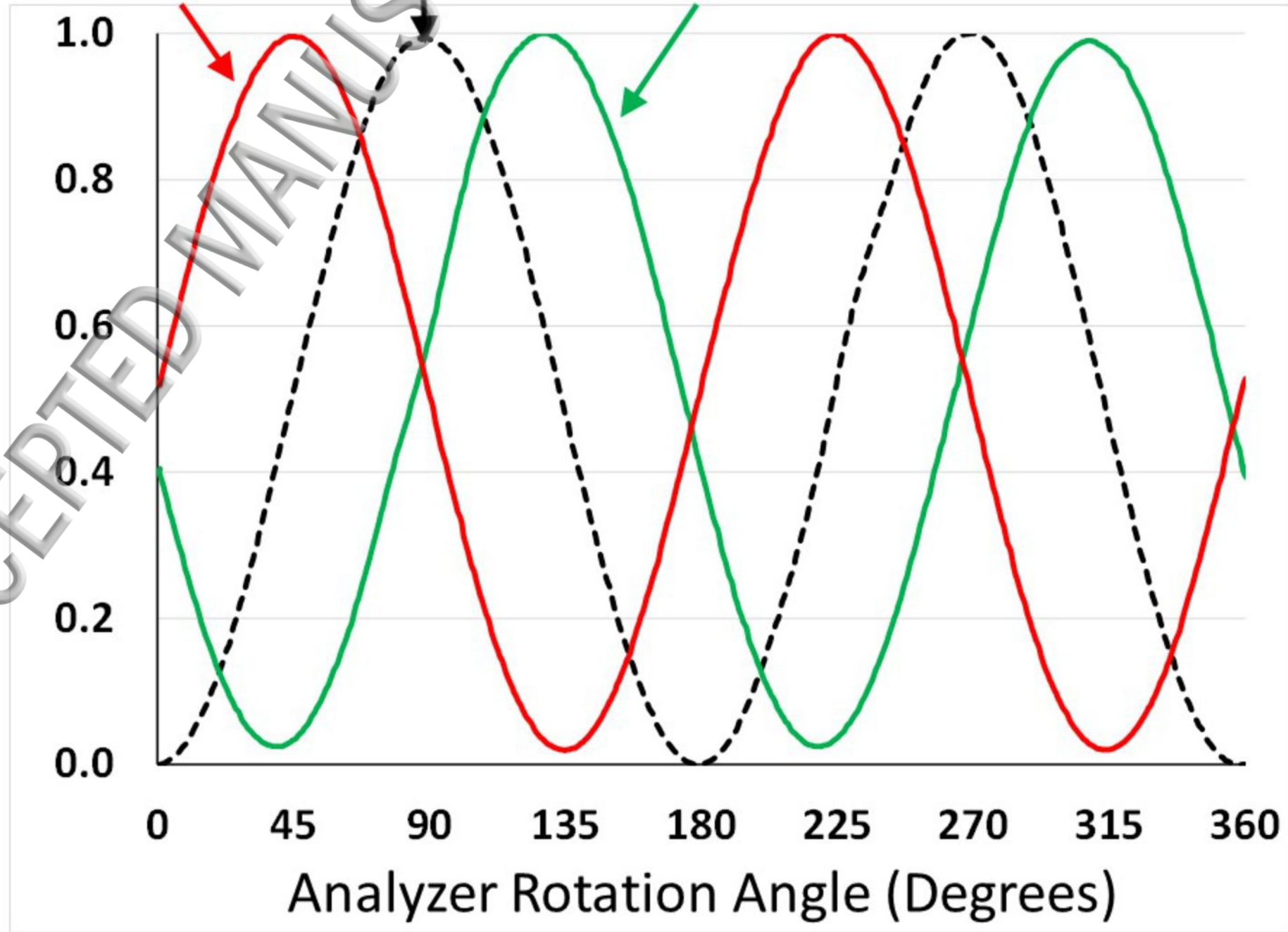

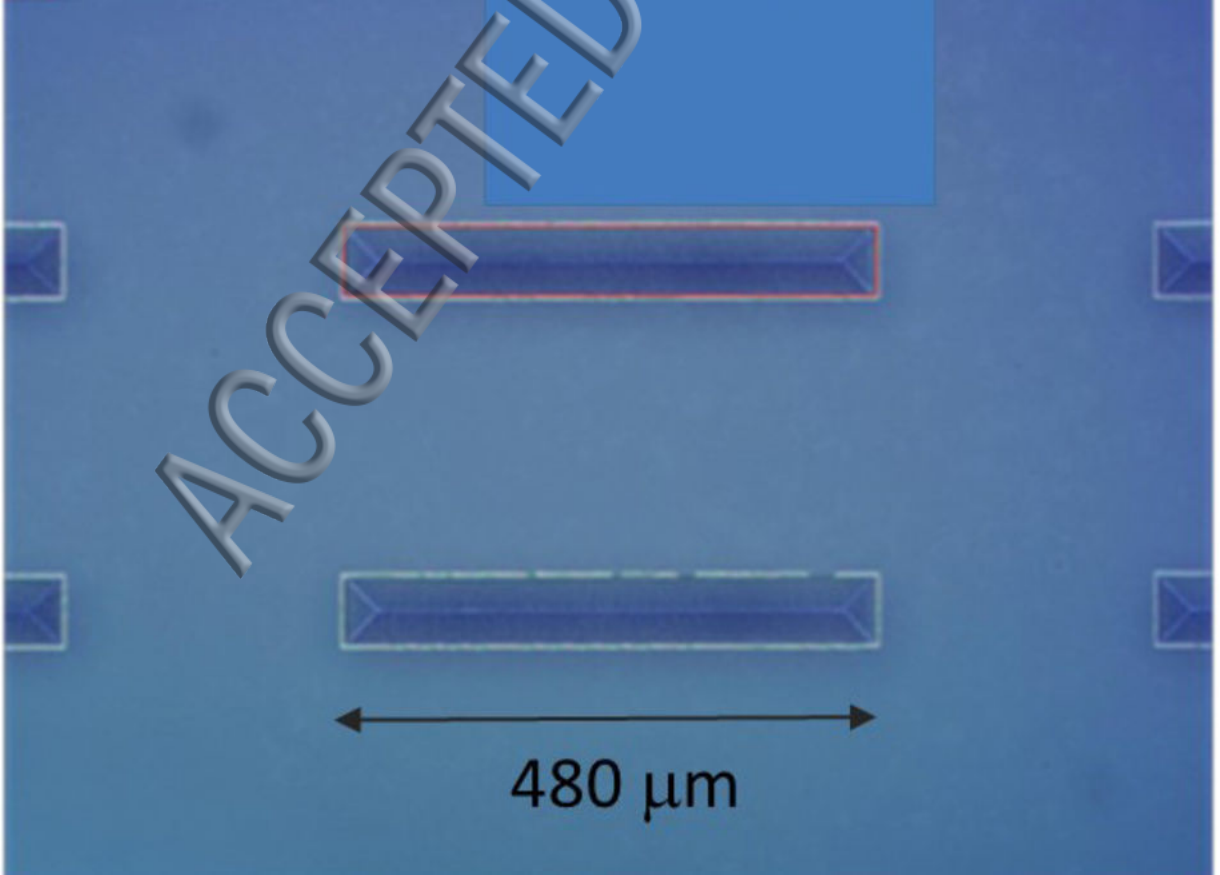

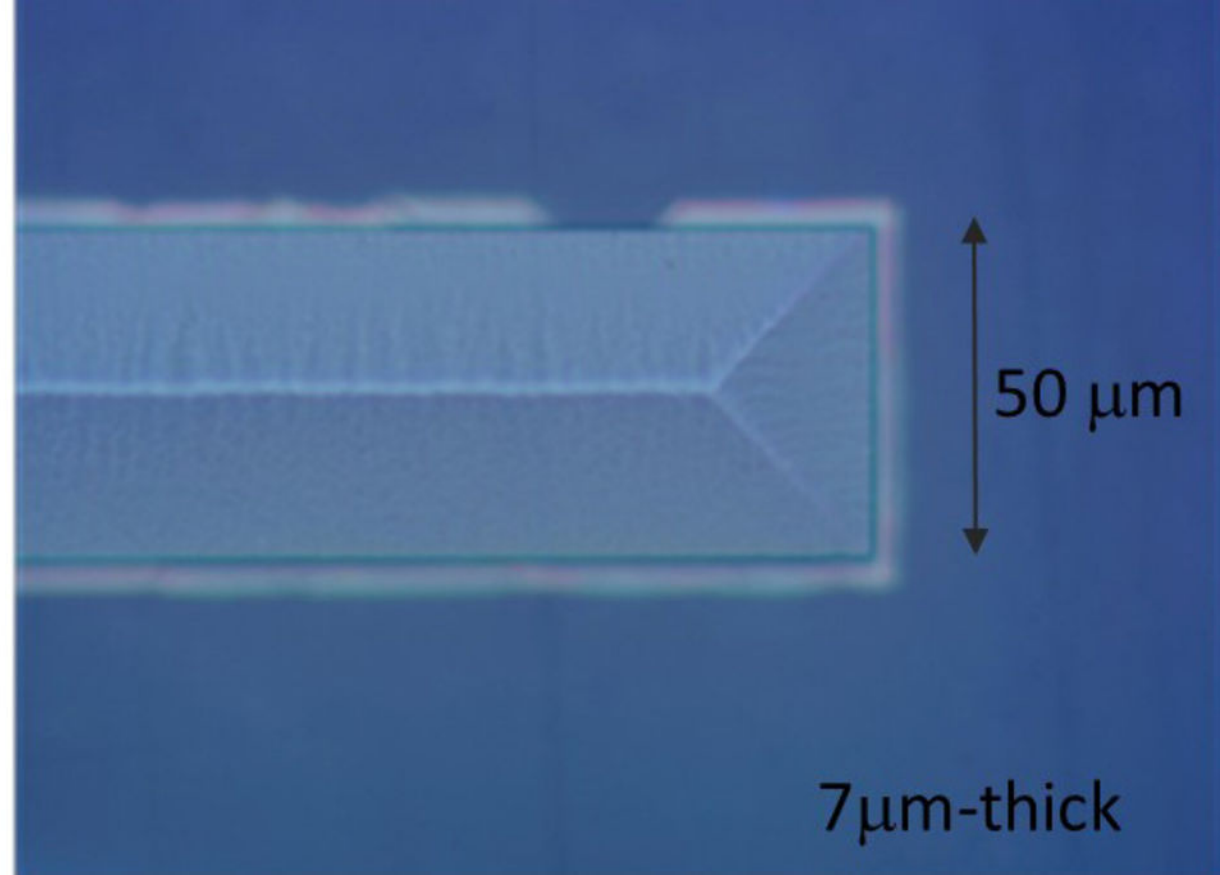

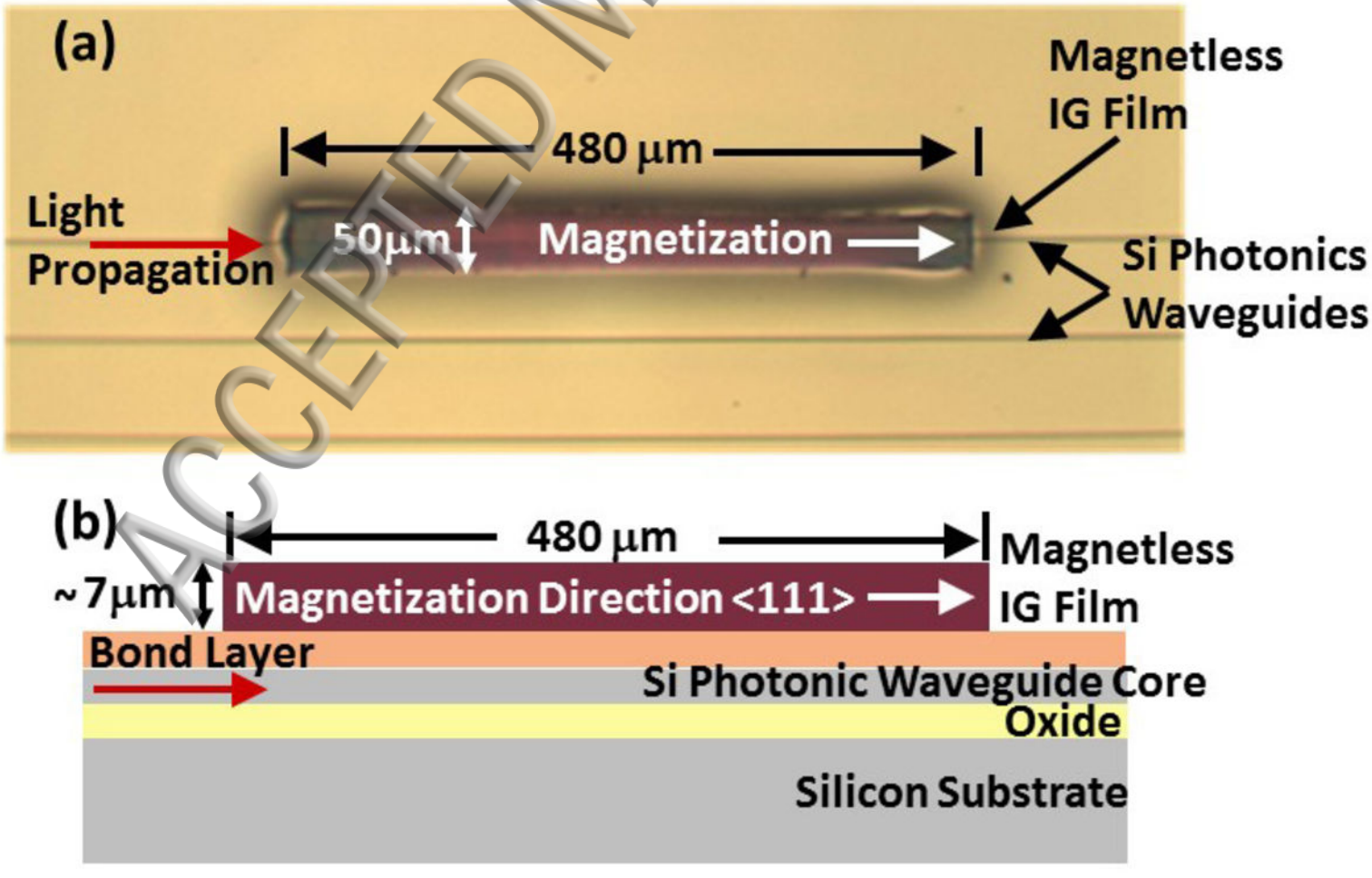
(a)
Magnetless
IG Film
480 μm
Light
Propagation
50μm
Magnetization
Si Photonics
Waveguides
(b)
480 μm
Magnetless
~7μm
Magnetization Direction <111>
IG Film
Bond Layer
Si Photonic Waveguide Core
Oxide
Silicon Substrate